

Absorption cross sections of *E,E*-2,4-hexadienedial at 248 nm, and in the 290–430 nm region, and photolysis study at 248, 308, and 351 nm

Bin Xiang, Lei Zhu *

Wadsworth Center, New York State Department of Health, Albany, NY 12201-0509, United States
Department of Environmental Health Sciences, State University of New York, Albany, NY 12201-0509, United States

Received 28 August 2007; in final form 5 November 2007

Available online 26 November 2007

Abstract

We have measured the absorption cross sections of *E,E*-2,4-hexadienedial at 248 nm and in the 290–430 nm region. The HCO product channel following 248, 308, and 351 nm photolysis of *E,E*-2,4-hexadienedial was examined. The HCO radical was only observed at 248 nm, with quantum yield of 0.014 (absolute uncertainty in HCO yield is ~86%). Estimated upper limits for the HCO yields at 308 and 351 nm are 11% and 9%. Acetylene, ketene, butadiene (all at 248 nm), CO (248 and 308 nm) have been detected as photolysis products of *E,E*-2,4-hexadienedial in 20 Torr of nitrogen. Their yields have been estimated.

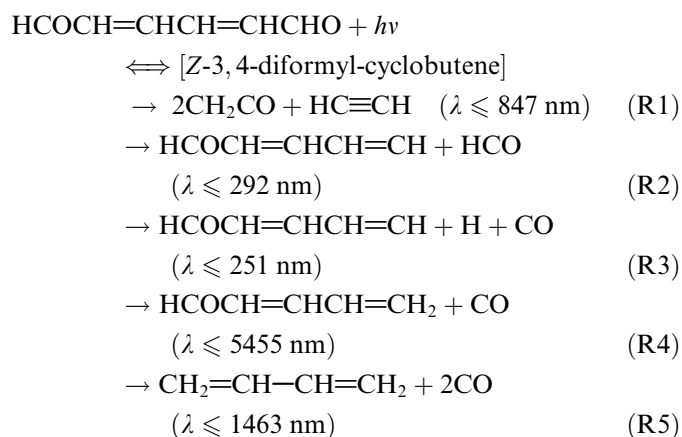
© 2007 Elsevier B.V. All rights reserved.

1. Introduction

E,E-2,4-Hexadienedial (HCOCH=CHCH=CHCHO) is a ring-cleavage product in the OH-initiated photooxidation of aromatic hydrocarbons [1–4]. *E,E*-2,4-Hexadienedial is highly toxic; it is a suspected carcinogen [5,6]. Photolysis and reaction with OH are its important atmospheric sinks [7,8]. The rate constant [8] for reaction of OH with *E,E*-2,4-hexadienedial was determined to be $(7.6 \pm 0.8) \times 10^{-11} \text{ cm}^3 \text{ molecule}^{-1} \text{ s}^{-1}$. The photolysis of *E,E*-2,4-hexadienedial has been investigated under smog-chamber conditions [7,8]. The mechanism [8] of the photolysis was proposed to involve the formation of a short-lived intermediate (a likely candidate is *Z*-3,4-diformyl-cyclobutene), followed by dissociation into the products. Photolysis of *E,E*-2,4-hexadienedial was also a source of secondary organic aerosol [8]. So far, only the estimated UV absorption cross section data are available for *E,E*-2,4-hexadienedial in the gas-phase, due to its low volatility (vapor

pressure ~4 mTorr at room temperature) and the difficulty in transferring it quantitatively to the gas-phase. Quantitative determination of the UV/visible absorption cross sections, photolysis product channels, and quantum yields of *E,E*-2,4-hexadienedial is necessary in order to elucidate the atmospheric photodissociation fates of *E,E*-2,4-hexadienedial and the atmospheric fates of aromatic hydrocarbons.

Photolysis of *E,E*-2,4-hexadienedial can occur through the following pathways:



* Corresponding author. Address: Wadsworth Center, New York State Department of Health, Albany, NY 12201-0509, United States. Fax: +1 518 473 2895.

E-mail address: zhul@wadsworth.org (L. Zhu).

where photochemical thresholds were calculated from the corresponding enthalpy changes [9]. Pathway (R1) is a ketene formation channel. Pathways (R2) and (R3) are radical formation channels. Pathways (R4) and (R5) are molecular elimination channels.

In this Letter, we report results obtained from absorption cross section measurements of *E,E*-2,4-hexadienedial at 248 nm and in the 290–430 nm region. The HCO radical was observed after 248 nm photolysis of *E,E*-2,4-hexadienedial, and its quantum yield has been determined. Ketene formation was observed at 248 nm photolysis wavelength. The end-product yields from 248 and 308 nm photolysis of *E,E*-2,4-hexadienedial have been estimated using FTIR.

2. Experimental technique

The absorption cross sections of *E,E*-2,4-hexadienedial in the 290–430 nm region were determined by cavity ring-down spectroscopy [10,11]. The cylindrical cell used for cross section measurements was 46 cm long; the two ends of the cell were sealed by a pair of high-reflectance cavity mirrors. Four pairs of high-reflectance cavity mirrors with centering wavelengths at 285 nm (covering 290–300 nm region), 320 nm (covering 300–340 nm region), 377 nm (covering 340–410 nm region), and 455 nm (covering 410–430 nm region) were used in the cross section measurements. The fundamental or the second harmonic output from a XeCl excimer-pumped dye laser (but at a much reduced fluence) was transmitted into the ring-down cavity through the front cavity mirror. The laser dyes used to cover the 290–430 nm region were rhodamin 6G, rhodamin B, rhodamin 101, DCM, PTP, BBQ, DPS, and stilbene 3. The photon intensity decay inside the cavity was monitored with a photomultiplier tube (PMT) placed behind the rear cavity mirror. The PMT output was amplified, digitized, and sent to a computer. The decay curve was fitted to a single-exponential decay function, from which the ring-down time constant (τ) and the total loss (Γ) per optical pass were calculated. When cavity mirrors were properly aligned, fitting of ring-down curve to single-exponential decay had a maximum uncertainty of 5%. By measuring the cavity losses with and without *E,E*-2,4-hexadienedial vapor in the cavity, we obtained optical loss due to *E,E*-2,4-hexadienedial absorption. Ring-down decay times for an empty cavity were about 0.79 μ s at 290 nm, 1.54 μ s at 320 nm, 0.42 μ s at 360 nm, and 1.17 μ s at 430 nm. With *E,E*-2,4-hexadienedial vapor in the cavity, ring-down decay times reduced to as low as 0.61 μ s at 290 nm, 1.30 μ s at 320 nm, 0.36 μ s at 360 nm, and 1.06 μ s at 430 nm. The gas pressure inside the cell was monitored by an MKS Baratron capacitance manometer (1 Torr full scale, pressure measurement accuracy is about 10^{-4} Torr), which can measure pressures down to 10^{-4} Torr. Before each experiment, the cell was pumped with a combination of rotary and diffusion pumps to 10^{-5} Torr. The cell had a degassing rate of 1×10^{-4} Torr/min in the absence of *E,E*-2,4-hexadienedial

sample. For cross section measurements, the pressure of *E,E*-2,4-hexadienedial vapor inside the cell was varied between 8×10^{-4} Torr and 4×10^{-3} Torr. The cell was evacuated before another pressure of *E,E*-2,4-hexadienedial was introduced into the cell to minimize the effect of outgassing. The cavity loss of the evacuated cell was about the same when going from one *E,E*-2,4-hexadienedial pressure to another suggesting that *E,E*-2,4-hexadienedial did not stick to the cavity mirrors. The cross section measurements were made under static condition, and the *E,E*-2,4-hexadienedial sample was stable (we did not observe deposit on the mirrors or in the absorption cell). An H NMR analysis described later in this section indicated that the *E,E*-2,4-hexadienedial sample had a minimum purity of $\geq 99.9\%$. It took up to 2 min. to fill 3×10^{-3} Torr of *E,E*-2,4-hexadienedial in the cell. Once the cell was filled with the sample, it took about 8 s to perform a ring-down measurement with a 1 Hz laser repetition rate and eight count average. Considering the cell degassing rate and the sample filling time, as well as the accuracy of pressure read-out, the maximum uncertainty in *E,E*-2,4-hexadienedial concentration measurement is estimated about 17%.

Photolysis of *E,E*-2,4-hexadienedial was carried out in a stainless steel cell. Detailed descriptions of our experimental setup can be found elsewhere [12–14]. The output from an excimer laser was propagated into the reaction cell at a 15° angle with the main cell axis, through a side arm. The probe laser beam, used to monitor the HCO radical generated from the photolysis process, was directed along the main optical axis of the cell; the cell had been vacuum-sealed with a pair of highly reflective cavity mirrors. The probe laser beam overlapped with the photolysis beam at the center of the cavity. The photolysis/probe laser overlap region can be conceptualized as a rectangular solid with its center overlapping that of the cell, with its width and height defined by those of the photolysis beam, and with the length of the rectangular solid defined by $(\text{beam width}) \times (\tan 15^\circ)^{-1}$, where 15° is the crossing angle between the pump and probe laser beams. The length of the photolysis/probe laser overlap region is defined by $(\text{beam width}) \times (\sin 15^\circ)^{-1}$. For a 12 mm wide photolysis beam, the length of the photolysis/probe laser overlap region is about 4.6 cm. The HCO absorption resulting from the photolysis of *E,E*-2,4-hexadienedial was obtained by measuring the cavity losses with and without photolysis in the 613–617 nm region ($\text{HCO } X^2A''(0,0,0) \rightarrow A^2A'(0,9,0)$ transition). A pulse/delay generator was used to vary the delay time between the firings of the photolysis and the probe lasers. The incident photolysis beam energy into the cell (E_0) was measured by a calibrated Joulemeter placed in front of the cell. The incident beam energy inside the cell was corrected for photolysis beam transmission loss at the front cell window, and for reflection of the photolysis beam from the rear cell window. *E,E*-2,4-Hexadienedial pressures of 6×10^{-4} – 3×10^{-3} Torr were used in the HCO quantum yield measurements. The end-products from 248 and 308 nm photolysis of *E,E*-2,4-hexadienedial

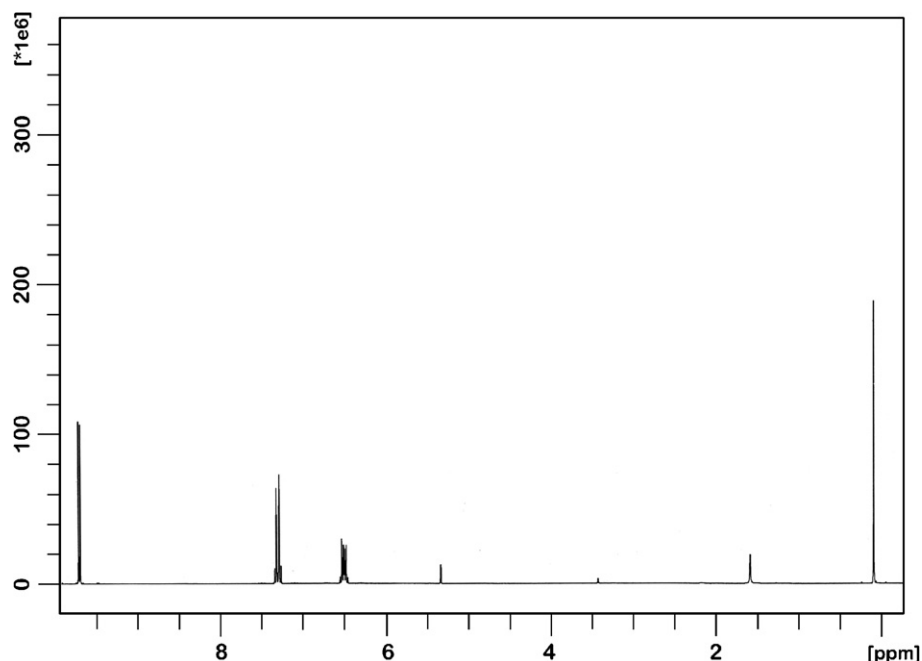


Fig. 1. ^1H NMR spectrum of our E,E -2,4-hexadienedial sample.

were determined using a Fourier-transform infrared spectrometer (Bruker IFS 66v).

E,E -2,4-Hexadienedial is a solid with a light-yellow color at 295 K. E,E -2,4-Hexadienedial was prepared using the procedure of Kossmehl and Bohn [15]. An ^1H NMR spectrum of E,E -2,4-hexadienedial is displayed in Fig. 1 with the following ^1H NMR (CDCl_2 , 5.32) peaks: 6.4665, 6.4740, 6.4865, 6.4955, 6.5033, 6.5150, 6.5225, 7.2527, 7.2725, 7.2801, 7.3018, 7.3094, 7.3293 (m, 4H, $\text{CH}=\text{CH}$), 9.6852, 9.7044 (d, 2H, CHO). The ^1H NMR analysis indicated that the E,E -2,4-hexadienedial sample had a minimum purity of $\geq 99.9\%$ (no impurity was detected in the NMR spectrum). Formaldehyde was generated by pyrolysis of paraformaldehyde ($\geq 95\%$ purity; Aldrich) at 110°C . All experiments were carried out at an ambient temperature of 295 ± 2 K.

3. Results and discussion

3.1. Absorption cross sections of E,E -2,4-hexadienedial at 248 nm and in the 290–430 nm region

We have determined the absorption cross sections of E,E -2,4-hexadienedial at 248 nm and in the 290–430 nm region. Absorption cross section at 248 nm was obtained by monitoring the transmitted photolysis fluence as a function of E,E -2,4-hexadienedial pressure in the cell, and by applying Beer's law. Absorption cross sections in the 290–430 nm region were determined by cavity ring-down spectroscopy. In the cavity ring-down cross section measurements, the absorption cross section at each wavelength was determined by measurement of the round-trip cavity losses due to absorption as a function of E,E -2,4-hexadi-

Table 1

Absorption cross sections (σ , in unit of $\text{cm}^2/\text{molecule}$) of E,E -2,4-hexadienedial as a function of wavelength (λ)

λ (nm)	σ	λ (nm)	σ
248	$(3.32 \pm 0.53^{\text{a,b}}) \times 10^{-17}$	360	$(9.53 \pm 0.38) \times 10^{-20}$
290	$(4.68 \pm 0.24^{\text{a,b}}) \times 10^{-19}$	365	$(1.00 \pm 0.07) \times 10^{-19}$
295	$(1.71 \pm 0.11) \times 10^{-19}$	370	$(9.50 \pm 0.73) \times 10^{-20}$
300	$(5.44 \pm 0.31) \times 10^{-20}$	375	$(8.88 \pm 0.39) \times 10^{-20}$
305	$(3.95 \pm 0.32) \times 10^{-20}$	380	$(9.24 \pm 0.05) \times 10^{-20}$
310	$(7.22 \pm 0.78) \times 10^{-20}$	385	$(7.38 \pm 0.30) \times 10^{-20}$
315	$(6.88 \pm 0.35) \times 10^{-20}$	390	$(6.26 \pm 0.18) \times 10^{-20}$
320	$(7.95 \pm 0.26) \times 10^{-20}$	400	$(5.05 \pm 0.17) \times 10^{-20}$
325	$(8.57 \pm 0.33) \times 10^{-20}$	405	$(3.66 \pm 0.70) \times 10^{-20}$
330	$(9.79 \pm 0.10) \times 10^{-20}$	410	$(3.43 \pm 0.12) \times 10^{-20}$
335	$(1.03 \pm 0.09) \times 10^{-19}$	415	$(3.11 \pm 0.05) \times 10^{-20}$
340	$(9.02 \pm 0.52) \times 10^{-20}$	420	$(2.16 \pm 0.11) \times 10^{-20}$
345	$(1.03 \pm 0.03) \times 10^{-19}$	425	$(1.43 \pm 0.14) \times 10^{-20}$
350	$(1.13 \pm 0.10) \times 10^{-19}$	430	$(8.07 \pm 1.63) \times 10^{-21}$
355	$(1.08 \pm 0.07) \times 10^{-19}$		

^a Errors quoted are standard deviations in the precision of the measurements.

^b Considering both relative errors and systematic errors, the overall uncertainty in the cross section measurements are within 25% at 320, 330, 345, 380, 390, 400, 410, 415 nm, 30% in the 290–305 and 360–375 nm region, and at 315, 325, 340, 355, 385, 420 nm, 35% at 310, 335, 350, 425 nm, 40% at 248 nm, 45% at 405, 430 nm.

enedial pressure in the cavity, and by plotting of the absorbance against E,E -2,4-hexadienedial pressure. Cross section data obtained are listed in Table 1 and shown in Fig. 2. As can be seen from Fig. 2, E,E -2,4-hexadienedial displays an absorption band in the 305–430 nm region (due to $n \rightarrow \pi^*$ transitions) and an absorption band at wavelengths less than 300 nm (due to $\pi \rightarrow \pi^*$ transitions). The absorption band at wavelengths less than 300 nm is

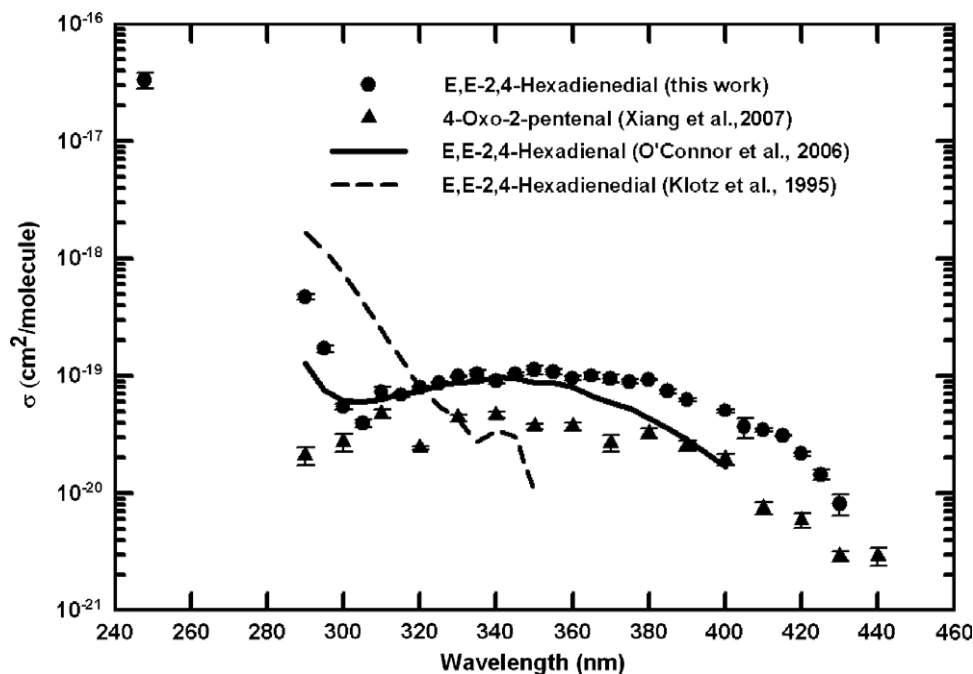


Fig. 2. Gas-phase absorption cross sections of *E,E*-2,4-hexadienedial (circles, this work; dashed line: [7]), *trans*-4-oxo-2-pentalenal (triangles, [16]) and *E,E*-2,4-hexadienal (solid line, [17]).

stronger than that in the longer-wavelength region. Cross section values of *E,E*-2,4-hexadienedial in the 305–430 nm region range from 8.1×10^{-21} to 1.1×10^{-19} cm²/molecule. Cross section values in the 290–300 nm region range from 5.4×10^{-20} to 4.7×10^{-19} cm²/molecule. The cross section value at 248 nm is $(3.32 \pm 0.53) \times 10^{-17}$ cm²/molecule. Klotz et al. [7] made qualitative cross section measurements on *E,E*-2,4-hexadienedial in the 220–355 nm region, and reported a cross section value of about 6×10^{-17} cm²/molecule at 248 nm. Since the cross section data obtained by Klotz et al. were reliable to within a factor of 2, our cross section value at 248 nm and theirs are consistent within the estimated uncertainty limits. However, there is a large difference between our cross section data and theirs in the 290–355 nm region. Their cross section data appeared to be limited by instrument detection sensitivity and a logarithm of their spectrum is shown in Fig. 2 for comparison.

Also shown in Fig. 2 for comparison with *E,E*-2,4-hexadienedial are absorption cross sections of 4-oxo-2-pentalenal [16] (CH₃COCH=CHCHO) and *E,E*-2,4-hexadienal [17] (CH₃CH=CH-CH=CHCHO). These unsaturated carbonyl/unsaturated dicarbonyls have conjugated π bonds and exhibit near UV absorption approaching 400 nm or longer-wavelengths. The peak cross section values for the $n \rightarrow \pi^*$ region of the absorption spectra for *E,E*-2,4-hexadienedial, *E,E*-2,4-hexadienal, and 4-oxo-2-pentalenal are 1.13×10^{-19} , 9.85×10^{-20} , and 4.76×10^{-20} cm²/molecule, respectively. Thus, it appears that cross section values in the near UV/visible region increase with increasing π conjugation. The near UV/visible band is broader for *E,E*-2,4-hexadienedial and 4-oxo-2-pentalenal than for

E,E-2,4-hexadienal, since the transitions arise from symmetric and antisymmetric combinations of the $n(\text{O})$ orbitals on the two carbonyl centers for unsaturated dicarbonyls.

3.2. Time-resolved studies of the photolysis of *E,E*-2,4-hexadienedial at 248, 308, and 351 nm

We investigated the photolysis of *E,E*-2,4-hexadienedial at 248, 308, and 351 nm, but we only observed the HCO radical at 248 nm photolysis wavelength. For HCO + CH=CH-CH=CH-CHO to be formed from the photolysis of *E,E*-2,4-hexadienedial, a C–C bond in the conjugated π system (O=C–C=C–C=C–C=O) must be broken. The lack of HCO product from the photolysis of *E,E*-2,4-hexadienedial at 308 and 351 nm is most likely the result of the higher photon energy required to break a C–C bond in the conjugated π system (The calculated photochemical threshold for this channel is 292 nm). The HCO radical was also not detected from the photolysis of another unsaturated dicarbonyl, 4-oxo-2-pentalenal, at either 308 or 351 nm [16].

The HCO quantum yield from the 248 nm photolysis of *E,E*-2,4-hexadienedial was derived from the ratio of the HCO concentration produced in the pump/probe laser overlap region to the absorbed photon density in the same region. The absorbed photolysis photon density in the pump/probe laser overlap region can be derived from the difference between the transmitted photolysis beam energies entering (E_{in}) and leaving (E_{out}) the overlap region, the individual photon energy (hc/λ) at the photolysis wavelength (λ), and the volume (v)

of the overlap region. The photolysis beam energy entering or leaving the pump/probe laser overlap region can be calculated from the incident photolysis beam energy entering the cell (E_0), the absorption cross section (σ) and the density (n) of *E,E*-2,4-hexadienedial in the cell, and the absorbing path length, by application of Beer's law:

$$E_{\text{in}} = E_0 \cdot \exp(-\sigma n l_1)$$

$$E_{\text{out}} = E_0 \cdot \exp(-\sigma n l_2)$$

where l_1 is the distance between the photolysis beam entrance and the beginning of the pump/probe laser overlap region, and l_2 is the distance between the photolysis beam entrance and the end of the pump/probe laser overlap region. The HCO concentration following the 248 nm photolysis of *E,E*-2,4-hexadienedial was obtained by measurement of HCO's absorption at 613.80 nm (HCO X²A'' (0,0,0) → A²A' (0,9,0) R bandhead) at a photolysis laser and a probe laser delay of 15 μs. The absolute HCO concentration was calibrated relative to the HCO concentration from the Cl + H₂CO → HCO + HCl reaction, with 248 nm photolysis of CCl₄ used as the Cl atom precursor. CCl₄ was freeze-pump-thawed and then mixed with formaldehyde in a gas manifold. The calibrated CCl₄/H₂CO mixture (P_{CCl₄}/P_{H₂CO} varied between 1/6 and 1/15) was transferred into a gas bulb before being introduced into the reaction cell. Partial pressures of CCl₄ and H₂CO inside the cell were calculated from their total pressure in the cell and their percentages in the mixture. The HCO absorption cross section at 613.80 nm obtained from the calibration experiments agreed within 24% with our previously reported [13] HCO absorption cross section of $\sim 2.0 \times 10^{-18}$ cm²/molecule at this wavelength. The dependence of the HCO quantum yields on nitrogen buffer gas pressure was examined over the pressure range covered by a 1 Torr full scale Baratron capacitance manometer (0.1–1.1 Torr); no dependence was observed. Increasing delay time between the firing of the photolysis and the probe laser also did not increase HCO yield. The average HCO quantum yield from the 248 nm photolysis of 0.0006–0.003 Torr of *E,E*-2,4-hexadienedial is 0.014 ± 0.002 , where the error quoted represents measurement precision. Systematic error in the determination of HCO quantum yield includes uncertainties in the determination of: HCO absorption cross section ($\sim 24\%$), *E,E*-2,4-hexadienedial concentration and absorption cross section ($\sim 40\%$ at 248 nm), pulse energy ($\sim 5\%$), and angle between photolysis and probe lasers (3%). With both random and systematic errors taken into account, the overall uncertainty (1σ measurement error plus systematic errors) in the determination of HCO quantum yield is about 86% at 248 nm.

The minimum round-trip HCO absorption that can be detected using our current cavity ring-down setup is 1 ppm. With a 12 mm wide excimer beam, the length of the photolysis/probe laser overlap region is 4.6 cm. The lack of detection of HCO at 308 and 351 nm photolysis wavelengths suggested that the HCO concentration in the

photolysis/probe laser overlap region was less than 5.4×10^{10} molecules/cm³. The incident photolysis fluences at 308 and 351 nm were about 0.043 and 0.024 J/cm². The absorbed photon densities from 308 and 351 nm photolysis of 0.004 Torr of *E,E*-2,4-hexadienedial were about 5.1×10^{11} and 6.2×10^{11} molecules/cm³. The lack of detection of HCO at 308 and 351 nm suggests the upper limits for the HCO yields are about 11% at 308 nm and 9% at 351 nm.

3.3. Photolysis end-product studies with FTIR at 248, 308, and 351 nm

We measured the infrared absorption spectrum of *E,E*-2,4-hexadienedial in the 500–4000 cm⁻¹ region. Shown in the upper panel of Fig. 3 is an IR absorption spectrum of 2 mTorr of *E,E*-2,4-hexadienedial (0.5 cm⁻¹ resolution); this spectrum agrees well with that reported previously for *E,E*-2,4-hexadienedial [7]. *E,E*-2,4-Hexadienedial was photolyzed in a stainless steel White cell (the pathlength used in the IR measurement was 6.7 m) mounted vertically in the sample compartment of a Bruker IFS66v FTIR spectrometer. The photolysis laser beam was introduced into the White cell through two rectangular fused silica windows (6" × 1.75") mounted on opposite side of the cell and it passed through the cell four times with the use of external reflectors. The end-products after 248, 308, and 351 nm photolysis of *E,E*-2,4-hexadienedial in 20 Torr of nitrogen carrier gas were analyzed using FTIR. Photolysis of *E,E*-2,4-hexadienedial was not observed at 351 nm even after photolyzing it for 2 h at a laser repetition rate of 2 Hz. The incident 351 nm photolysis fluence was about 0.0013 J/cm². With 2 mTorr of *E,E*-2,4-hexadienedial in the multi-pass cell, using the absorption cross section of *E,E*-2,4-hexadienedial of 1.12×10^{-19} molecules/cm² at 351 nm and correcting for photolysis transmission losses at the surfaces of mirrors and windows, the total number of 351 nm photolysis photon absorbed by *E,E*-2,4-hexadienedial after 2 h photolysis was about 2.1×10^{16} photons. The cell volume is about 2.3 l. The absorbed photolysis photon density averaged over the cell volume was about 10^{13} photons/cm³ (the absorbed photolysis photon density in the excimer laser path inside the White cell was larger than the absorbed photolysis photon density averaged over the cell volume). We should be able to detect either loss of reactant or appearance of products if *E,E*-2,4-hexadienedial were photolyzed at 351 nm. *E,E*-2,4-Hexadienedial photolyzed rapidly at 248 nm. Presented in the lower panel of Fig. 3 is an FTIR difference spectrum obtained by subtraction of the FTIR spectrum following 10 min photolysis of *E,E*-2,4-hexadienedial at 248 nm by the reactant spectrum. The products that were detected following 248 nm photolysis of *E,E*-2,4-hexadienedial include CO, ketene, butadiene, and acetylene (CO₂ is likely an artifact resulting from reaction at the wall). CO was identified by its IR absorption in the 2030–2240 cm⁻¹ region. An expanded product spectrum in the 2030–2240 cm⁻¹ region clearly

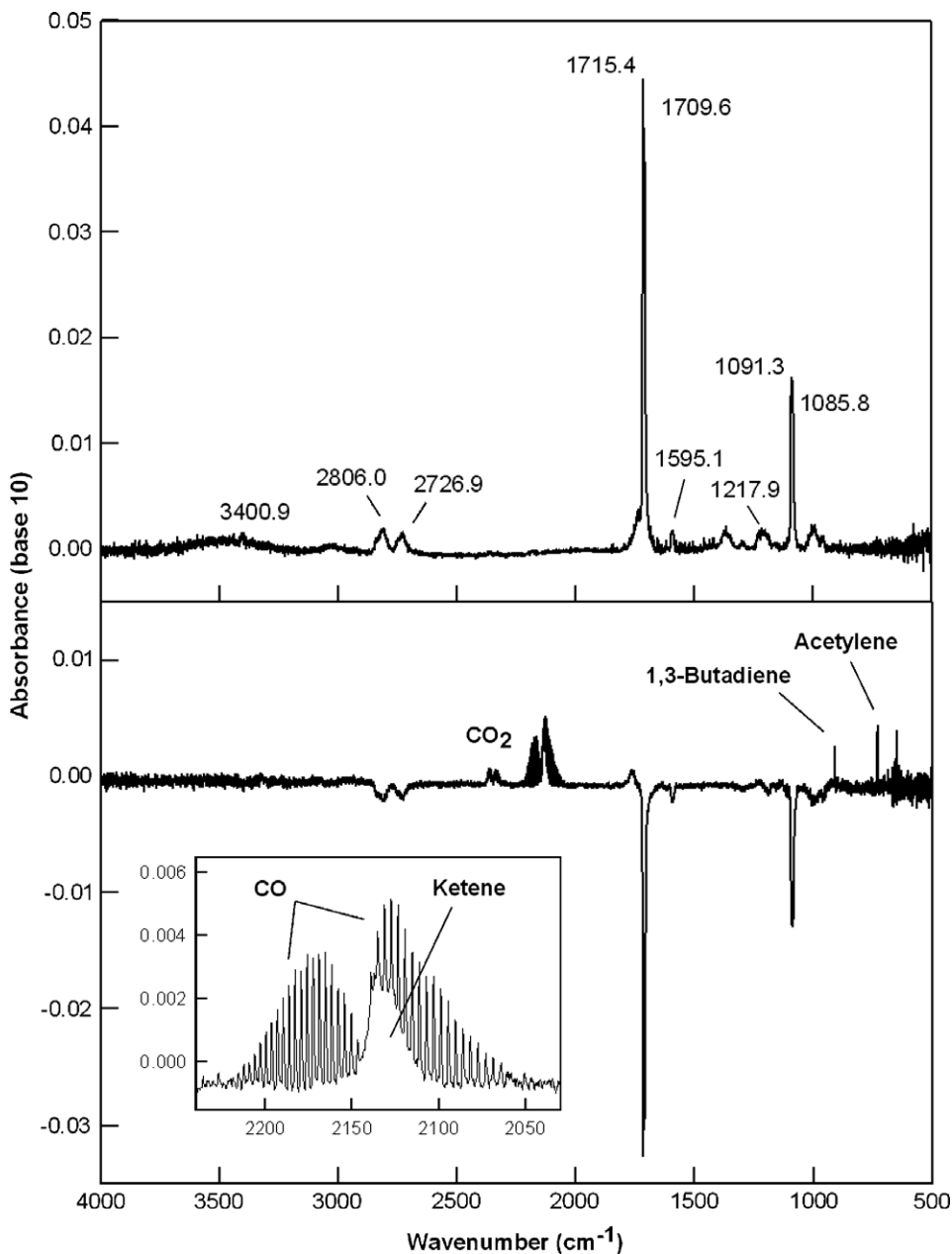
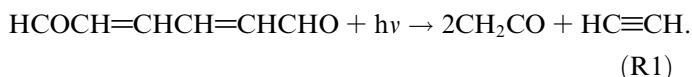
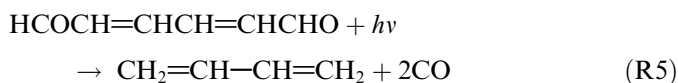
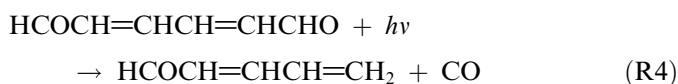


Fig. 3. (Upper panel) FTIR spectrum of 0.002 Torr of *E,E*-2,4-hexadienedial in the absence of photolysis. (Lower panel) FTIR difference spectrum after 248 nm photolysis of 0.002 Torr *E,E*-2,4-hexadienedial in 20 Torr of nitrogen for 10 min.

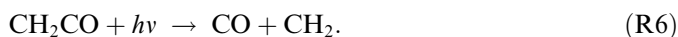
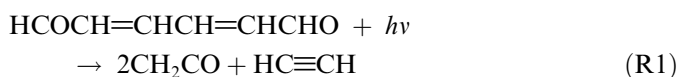
showed that a broad IR contour peaking at 2131.5 cm^{-1} was buried under the R-branch of the CO band. This broad IR band can be attributed to that of ketene. Butadiene was identified by its IR absorption peak at 908.1 cm^{-1} . Acetylene was identified by its IR absorption at 729.2 cm^{-1} . CO was also detected from the 308 nm photolysis of *E,E*-2,4-hexadienedial. Ketene is possibly a product of the *E,E*-2,4-hexadienedial photolysis channel:



CO can be a product of the *E,E*-2,4-hexadienedial photolysis channels:

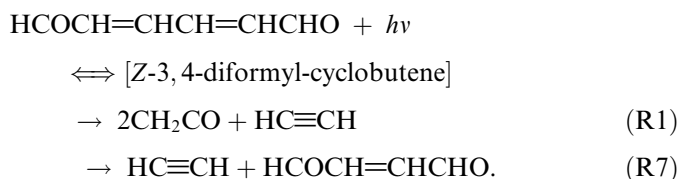


where butadiene is a co-product of the photolysis channel (5). CO can also be a secondary photolysis product of *E,E*-2,4-hexadienedial:



By comparing the CO and the ketene formed from the 248 nm photolysis of *E,E*-2,4-hexadienedial as a function of photolysis time, we found that the amount of CO formed initially increased with photolysis time and then leveled-off while the amount of ketene formed initially decreased with photolysis time and then leveled-off, suggesting at least part of the CO is formed from ketene photolysis. Threshold wavelength for ketene photolysis to form ${}^1\text{CH}_2 + \text{CO}$ was previously reported to be around 332 nm [18].

Acetylene is likely formed from the *E,E*-2,4-hexadienedial photolysis channels:



Unfortunately, the overlapping IR absorption between the butenedial formed from the photolysis and the unphotolyzed *E,E*-2,4-hexadienedial prevented us from monitoring butenedial product by the IR method. In addition, butenedial can be photolyzed by 248 nm radiation.

By using the sample standards to calibrate the photolysis products' IR spectra and by dividing the mole number of products formed by the mole number of photolyzed *E,E*-2,4-hexadienedial, we obtained the estimated yields of acetylene, butadiene, and CO from the photolysis of *E,E*-2,4-hexadienedial. Photolysis times were varied so that 20–90% of the *E,E*-2,4-hexadienedial was photolyzed. Since the IR absorption cross section of the ketene is not known, we did not correct for the formation of CO from the secondary photolysis of ketene. The sum of the yields of all *E,E*-2,4-hexadienedial photolysis channels should be equal to 1. Since the photolysis of *E,E*-2,4-hexadienedial can lead to the formation of two CO, the end-product yield of CO can be expected to be in the range of 0 and 2. The estimated yields of CO from the photolysis of *E,E*-2,4-hexadienedial at 248 and 308 nm are about 150% and 151%. Yields of acetylene and butadiene from the 248 nm photolysis of *E,E*-2,4-hexadienedial are ~59% and ~23%. The quantum yields of the products were estimated by dividing the mole number of the products formed by the mole number of photons absorbed by *E,E*-2,4-hexadienedial. The estimated quantum yields of CO from the photolysis of *E,E*-2,4-hexadienedial at 248 and 308 nm are about 112% and 97%. The estimated quantum yields of acetylene and butadiene from the 248 nm photolysis of *E,E*-2,4-hexadienedial are about 32% and 14%. The estimated quantum yields are smaller than the estimated photolysis end-product yields as photolysis intermediates can also absorb photolysis photons, plus the fact it was a static photolysis system and the reactant did not get replenished from each laser pulse. Thus, we over-estimated photon density absorbed by *E,E*-2,4-hexadienedial in the quantum yield calculation.

3.4. Atmospheric photolysis rate constant for *E,E*-2,4-hexadienedial

We have estimated the atmospheric photolysis rate constants ($k_{\text{photolysis}}$) of *E,E*-2,4-hexadienedial using the following formula:

$$k_{\text{photolysis}} = \Sigma \sigma(\lambda) \cdot \varphi(\lambda) \cdot J(\lambda) \Delta\lambda$$

where $J(\lambda)$ represents actinic solar flux, $\sigma(\lambda)$ represents the gas-phase absorption cross sections of *E,E*-2,4-hexadienedial determined in this work, and $\varphi(\lambda)$ represents the photolysis quantum yield for *E,E*-2,4-hexadienedial. $J(\lambda)\Delta\lambda$ values reported by Demerjian et al. [19] were used. In the photolysis rate calculation, $\varphi(\lambda)$ was assumed to be unity in the 290–310 nm region, 0 at 350 nm, and $\varphi(\lambda)$ in the 310–350 nm region was assumed to decrease linearly from 1 at 310 nm to 0 at 350 nm. $\varphi(\lambda)$ may not vary linearly with wavelength in the 310–350 nm region; we made this assumption solely for the simplicity in photolysis rate estimation. The photolysis rate constants for *E,E*-2,4-hexadienedial were estimated as a function of the zenith angle under cloudless conditions, at sea level, and for best-estimate albedo [20] (5% in the 290–350 nm region); the results are shown in Fig. 4. Our estimated photolysis rate constants for *E,E*-2,4-hexadienedial for zenith angles in the 0–60° range are 2.1×10^{-4} to $1.0 \times 10^{-4} \text{ s}^{-1}$; these values correspond to photolysis lifetimes of 1.3–2.8 h. Rate constants for *E,E*-2,4-hexadienedial reactions with OH and O₃ have been reported [7,8] to be 7.6×10^{-11} and $1 \times 10^{-17} \text{ cm}^3 \text{ molecule}^{-1} \text{ s}^{-1}$, respectively. With a 12-h average OH concentration [21,22] of $1.6 \times 10^6 \text{ molecule/cm}^3$, and a 24-h average O₃ concentration [23] of $7 \times 10^{11} \text{ molecule/cm}^3$, the *E,E*-2,4-hexadienedial reaction

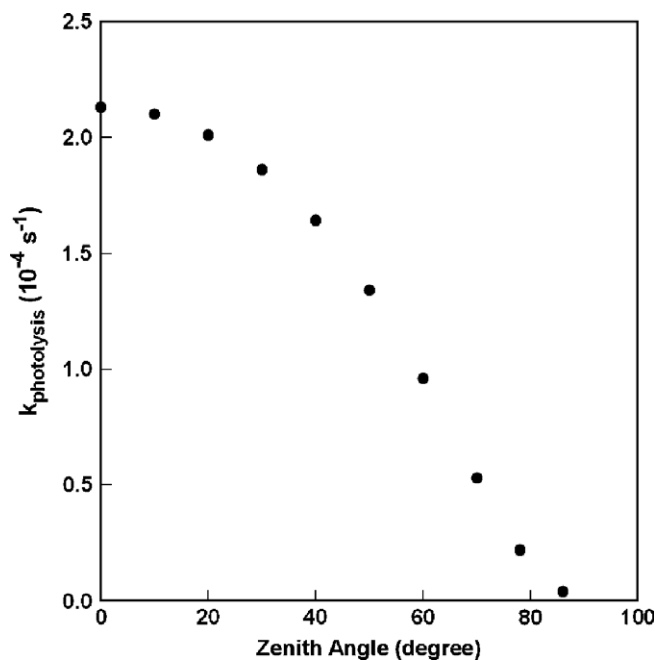


Fig. 4. Calculated atmospheric photolysis rate constants of *E,E*-2,4-hexadienedial as a function of solar zenith angle.

lifetimes with OH and O₃ are 2.3 h and 1.7 days, respectively. Thus, photolysis and OH radical reactions are major processes for removal of *E,E*-2,4-hexadienedial from the atmosphere.

Acknowledgements

We are indebted to Dr. Gisela Witz (UMDNJ-Robert Wood Johnson Medical School) for kindly providing us *E,E*-2,4-hexadienedial sample used in this study. We thank Dr. Chengzhu Zhu for his help with the experiments, Lynn McNaughton at the CoreNMR Facility of the Wadsworth Center for performing H NMR characterization of *E,E*-2,4-hexadienedial samples. Discussion with Dr. Ted Dibble about bond energy calculation is acknowledged. We are grateful for the support provided by the National Science Foundation under Grant #ATM-0300294.

References

- [1] B. Klotz, I. Barnes, K.H. Becker, B.T. Golding, *J. Chem. Soc. Faraday Trans.* 93 (1997) 1507.
- [2] B.E. Dumdei, R.J. O'Brien, *Nature* 311 (1984) 248.
- [3] B.E. Dumdei, D.V. Kenney, P.B. Shepson, T.E. Kleindienst, C.M. Nero, L.T. Cupitt, L.D. Claxton, *Environ. Sci. Technol.* 22 (1988) 1493.
- [4] J. Yu, H.E. Jeffries, K.G. Sexton, *Atmos. Environ.* 31 (1997) 2261.
- [5] G. Witz, G.S. Rao, B.D. Goldstein, *Toxicol. Appl. Pharmacol.* 80 (1985) 511.
- [6] C. Bleasdale, B.T. Golding, G. Kennedy, J.O. MacGregor, W.P. Watson, *Chem. Res. Toxicol.* 6 (1993) 407.
- [7] B.G. Klotz, A. Bierbach, I. Barnes, K.H. Becker, *Environ. Sci. Technol.* 29 (1995) 2322.
- [8] B. Klotz, I. Barnes, K.-H. Becker, *Int. J. Chem. Kinet.* 31 (1999) 689.
- [9] D.R. Lide (Ed.), *CRC Handbook of Chemistry and Physics*, CRC Press, Boca Raton, FL, 2007.
- [10] A. O'Keefe, D.A.G. Deacon, *Rev. Sci. Instrum.* 59 (1988) 2544.
- [11] A. O'Keefe, J.J. Scherer, A.L. Cooksy, R. Sheeks, J. Heath, R.J. Saykally, *Chem. Phys. Lett.* 172 (1990) 214.
- [12] T.J. Cronin, L. Zhu, *J. Phys. Chem. A* 102 (1998) 10274.
- [13] Y. Tang, L. Zhu, *J. Phys. Chem. A* 108 (2004) 8307.
- [14] L. Zhu, G. Johnston, *J. Phys. Chem.* 99 (1995) 15114.
- [15] G. Kossmehl, B. Bohn, *Chem. Ber.* 107 (1974) 710.
- [16] B. Xiang, L. Zhu, Y. Tang, *J. Phys. Chem. A* 111 (2007) 9025.
- [17] M.P. O'Connor, J.C. Wenger, A. Mellouki, K. Wirtz, A. Munoz, *Phys. Chem. Chem. Phys.* 8 (2006) 5236.
- [18] C.-K. Ni, E.A. Wade, M.V. Ashikhmin, C.B. Moore, *J. Mol. Spectrosc.* 177 (1996) 285.
- [19] K.L. Demerjian, K.L. Schere, J.T. Peterson, *Adv. Environ. Sci. Technol.* 10 (1980) 369.
- [20] K.L. Coulson, D.W. Reynolds, *J. Appl. Meteorol.* 10 (1971) 1285.
- [21] R. Prinn et al., *J. Geophys. Res.* 97 (1992) 2445.
- [22] P.J. Crutzen, P.H. Zimmermann, *Tellus* 43AB (1991) 136.
- [23] J.A. Logan, *J. Geophys. Res.* 90 (1985) 10463.